©SHUTTERSTOCK.COM/NAYPONG STUDIO

Fully Actuated Multirotor UAVs

A Literature Review

By Ramy Rashad, Jelmer Goerres, Ronald Aarts, Johan B.C. Engelen, and Stefano Stramigioli

In the last decade, the aerial robotics community has witnessed an increased interest in fully actuated multirotor unmanned aerial vehicles (UAVs) that have more capabilities than conventional underactuated multirotors. This article collects the different UAV designs having fully actuated aerodynamic wrench generation proposed in the literature to date. The work includes a systematic derivation of the control–allocation matrix for all of the concepts as well as a discussion of the different quantitative criteria used for optimizing UAV designs.

Digital Object Identifier 10.1109/MRA.2019.2955964
Date of current version: 31 January 2020

Conventional Multirotor UAVs

UAVs have seen great growth in popularity. They have facilitated cost-effective engineering solutions in many civilian applications by enabling various sensors to be deployed in the air. Multirotor UAVs have been widely used due to their unique qualities, such as vertical takeoff and landing, hovering, and mechanical simplicity. Conventional multirotor UAV designs, including the quadrotor and hexarotor, are optimized for maximum flight time. All such UAV rotors have parallel directions to collectively counteract gravity. Consequently, conventional multirotor UAVs have underactuated dynamics due to the coupling between the horizontal translational and rotational dynamics.

1070-9932/20©2020IEEE

For many applications, the underactuation property of the conventional designs has been alleviated by the use of gimbals to mount sensors onboard. However, the applicability of multirotor UAVs could be extended if full actuation can be achieved. An example of such applications is the emerging field of aerial physical interaction [1], in which UAVs are not required to act just as flying sensors but as airborne manipulators. Several fully actuated multirotor platforms were introduced during the past decade to overcome the underactuation property of conventional multirotors. Full actuation has been realized mainly by using fixed propellers with dissimilar orientations, which we refer to as *fixed-tilt concepts*, and actively tilting the propellers using extra actuators, which we refer to as *variable-tilt concepts*.

Multirotor UAVs have been widely used due to their unique qualities, such as vertical takeoff and landing, hovering, and mechanical simplicity.

The problem with fully actuated UAV concepts is that the optimal rotor configuration is application-dependent, contrary to underactuated concepts, which usually have the orientation of their rotors in a vertical in-plane symmetric configuration. To achieve full actuation, the orientation and location of the rotors must be altered, which results in a wide range of possible configurations. Depending on the requirements of the application, a vast variety of different concepts results.

Background

In this section, we show how to derive the control-allocation matrix, which maps the UAV control inputs (that is, the propellers' thrust) to the total aerodynamic wrench applied to the UAV's body. This is done by defining the reference frames, followed by a static wrench analysis and the classification of multirotor UAVs based on the mapping matrix. For a more comprehensive introduction to the topic, readers are referred to textbooks such as [2] and [3].

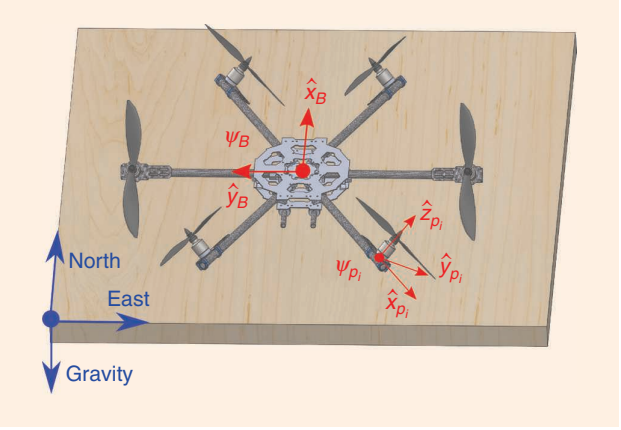

Figure 1. A schematic view of the reference frames used, illustrated on a fully actuated hexarotor.

Coordinate Frames

First, we introduce the notion of a coordinate frame, which is represented by the quadruple $\{\Psi_i : o_i, \hat{\boldsymbol{x}}_i, \hat{\boldsymbol{y}}_i, \hat{\boldsymbol{z}}_i\}$, where o_i represents the origin of the frame and $(\hat{\boldsymbol{x}}_i, \hat{\boldsymbol{y}}_i, \hat{\boldsymbol{z}}_i)$ is a triad of (right) mutually orthonormal basis vectors. Let $\{\Psi_B : o_B, \hat{\boldsymbol{x}}_B, \hat{\boldsymbol{y}}_B, \hat{\boldsymbol{z}}_B\}$ denote a body-fixed frame with o_B attached to the center of mass (CoM); $\hat{\boldsymbol{z}}_B$ is chosen such that gravity acts oppositely when the UAV rests on flat ground, and $\hat{\boldsymbol{x}}_B$ represents the UAV's forward direction so that, when the craft aligns to north, $\hat{\boldsymbol{y}}_B$ points west, as shown in Figure 1.

Associated with the ith propeller is the frame $\{\Psi_{p_i} : o_{p_i}, \hat{\boldsymbol{x}}_{p_i}, \hat{\boldsymbol{y}}_{p_i}, \hat{\boldsymbol{z}}_{p_i}\}$, where the origin, o_{p_i}, coincides with the CoM of the ith rotor and $\hat{\boldsymbol{z}}_{p_i}$ is oriented to the direction of the generated thrust (that is, normal to the spinning-disk area). The axis, $\hat{\boldsymbol{x}}_{p_i}$, is chosen so that it is collinear to the line connecting o_B to o_{p_i}, while $\hat{\boldsymbol{y}}_{p_i}$ completes the right-oriented triad, as depicted in Figure 1. The propeller frame, Ψ_{p_i}, does not rotate with the propeller; that is, for fixed-tilt concepts, it is attached to the body. However, for variable-tilt concepts, $\hat{\boldsymbol{z}}_{p_i}$ is always aligned with the variable thrust-generation direction.

With the aforementioned definitions of the coordinate frames, the configuration of each rotor/propeller can be determined by the displacement vector, $\boldsymbol{\xi}_i \in \mathbb{R}^3$, and orientation vector, $\boldsymbol{u}_i \in \mathbb{S}^2$, given by

$$\boldsymbol{\xi}_i := \boldsymbol{o}_{p_i}^B, \qquad \boldsymbol{u}_i(t) := \boldsymbol{R}_{p_i}^B(t)\hat{\boldsymbol{z}}, \tag{1}$$

where $\boldsymbol{o}_{p_i}^B \in \mathbb{R}^3$, $\boldsymbol{R}_{p_i}^B \in SO(3)$ denotes the position and orientation of Ψ_{p_i} with respect to Ψ_B and $\hat{\boldsymbol{z}} = (0, 0, 1)^\top$. The explicit time dependence in (1) is for variable-tilt UAVs, whereas for fixed-tilt UAVs, $\boldsymbol{\xi}_i$ and $\boldsymbol{u}_i$ are constants.

In the case of a planar multirotor (that is, a design with coplanar rotor positions) it is possible to parametrize the orientation matrix $\boldsymbol{R}_{p_i}^B$ by three angles such that

$$\boldsymbol{R}_{p_i}^B = \boldsymbol{R}_z(\psi_i)\boldsymbol{R}_y(\beta_i)\boldsymbol{R}_x(\alpha_i), \tag{2}$$

where $\boldsymbol{R}_k(\cdot)$ is the standard rotation matrix around the kth axis, while the angles α_i and β_i uniquely define the direction of thrust-generation axis $\hat{\boldsymbol{z}}_{p_i}$ in Ψ_B. The angle ψ_i denotes the heading, while α_i, β_i will be referred to, respectively, as the *cant and dihedral angles*.

Static-Control Wrench Analysis

The aerodynamic wrench produced by the rotors can be derived through a static analysis. A wrench represents the generalized force acting on a rigid body and consists of linear-force, $\boldsymbol{f} \in \mathbb{R}^3$, and rotational-torque, $\boldsymbol{\tau} \in \mathbb{R}^3$, components. A wrench applied to the origin of Ψ_i with its components specified in Ψ_i is denoted by $\boldsymbol{W}^i = (\boldsymbol{\tau}^{i\top}, \boldsymbol{f}^{i\top})^\top$. The change of a

wrench's coordinates between any two frames Ψ_i and Ψ_k can be performed by

$$\boldsymbol{W}^k = \boldsymbol{A}_i^k \boldsymbol{W}^i, \quad \boldsymbol{A}_i^k := \begin{pmatrix} \boldsymbol{R}_i^k & \tilde{\boldsymbol{o}}_i^k \boldsymbol{R}_i^k \\ \boldsymbol{0} & \boldsymbol{R}_i^k \end{pmatrix}, \tag{3}$$

where $\boldsymbol{o}_i^k$, $\boldsymbol{R}_i^k$ denotes the position and orientation of Ψ_i with respect to Ψ_k. The skew-symmetric matrix $\tilde{\boldsymbol{o}}$ in (3) is defined such that $\tilde{\boldsymbol{o}}\boldsymbol{x} = \boldsymbol{o} \wedge \boldsymbol{x}$, $\forall \boldsymbol{x} \in \mathbb{R}^3$, where $\wedge$ denotes the cross product on $\mathbb{R}^3$. In differential geometric terms, the matrix $\boldsymbol{A}_i^k$ represents the dual of the group adjoint operator, while $\boldsymbol{W}^i$ represents the Plucker coordinates of the wrench screw. For a more rigorous mathematical formulation, interested readers are referred to [4].

It is well known from the aerial-robotics literature that, in quasi-static flights, the aerodynamic thrust and drag torque of a propeller are approximately proportional to the square of the propeller's spinning velocity [5]. This simple aerodynamic-wrench model neglects many high-order effects, such as blade flapping and induced drag, that induce forces in the $\hat{\boldsymbol{x}}_{p_i}$-$\hat{\boldsymbol{y}}_{p_i}$ plane. However, for the scale of the multirotor UAVs used in robotics, these effects cause minor perturbations and are usually neglected in the control-design process [5]. Thus, the aerodynamic-wrench generation direction is along $\hat{\boldsymbol{z}}_{p_i}$ only.

The thrust magnitude generated by the ith propeller in Ψ_{p_i} is denoted by λ_i, while the drag torque is expressed as $\tau_{d,i} = \gamma\sigma_i\lambda_i$, where γ is the propeller's drag-to-thrust ratio, and $\sigma_i \in \{-1, 1\}$ specifies the propeller's rotation direction (with $\sigma_i = 1$ for clockwise rotation). The individual aerodynamic wrench generated from the ith propeller, applied to the UAV's body at the origin of Ψ_{p_i}, is expressed in Ψ_{p_i} as

$$\boldsymbol{W}_c^{p_i} = \lambda_i (0, 0, \gamma\sigma_i, 0, 0, 1)^\top. \tag{4}$$

By summing over i, the cumulative aerodynamic-control wrench, $\boldsymbol{W}_c^B$, from the total number of rotors, N_p, expressed in Ψ_B, can be written as

$$\boldsymbol{W}_c^B = \sum_i^{N_p} \boldsymbol{A}_{p_i}^B \boldsymbol{W}_c^{p_i}, \tag{5}$$

which can be expanded as

$$\begin{aligned} \begin{pmatrix} \boldsymbol{\tau}_c^B \\ \boldsymbol{f}_c^B \end{pmatrix} &= \sum_i^{N_p} \lambda_i \begin{pmatrix} \boldsymbol{R}_{p_i}^B & \tilde{\boldsymbol{\xi}}_i \boldsymbol{R}_{p_i}^B \\ \boldsymbol{0} & \boldsymbol{R}_{p_i}^B \end{pmatrix} \begin{pmatrix} \gamma\sigma_i \hat{\boldsymbol{z}} \\ \hat{\boldsymbol{z}} \end{pmatrix}, \\ &= \sum_i^{N_p} \lambda_i \begin{pmatrix} \gamma\sigma_i \boldsymbol{u}_i + \boldsymbol{\xi}_i \wedge \boldsymbol{u}_i \\ \boldsymbol{u}_i \end{pmatrix}, \end{aligned} \tag{6}$$

where the definitions in (1) have been used. We can rewrite (6) in a compact form as

$$\boldsymbol{W}_c^B = \boldsymbol{M}\boldsymbol{\lambda}, \tag{7}$$

where $\boldsymbol{\lambda} = (\lambda_1, \ldots, \lambda_{N_p})^\top \in \Lambda$ is the rotors' thrust vector and $\boldsymbol{M} \in \mathbb{R}^{6 \times N_p}$ is the control allocation/distribution matrix.

Classification of Multirotor UAVs

As shown in (7), the UAV's rotor configuration defines the mapping matrix, $\boldsymbol{M}$, which maps the allowable propeller–thrust space, Λ, to the allowable aerodynamic-control wrench space, $\mathbb{W}$. For fixed-tilt UAV designs, $\boldsymbol{M}$ is a constant matrix; for variable-tilt designs, it is a function of N_a angles representing the number of additional actuators used to actively tilt the propellers.

For the fixed-tilt design concept, the UAV can be classified as follows. If $rank(\boldsymbol{M}) < 6$, the UAV is said to be underactuated; if $rank(\boldsymbol{M}) = 6$ and $N_p = 6$, the UAV is fully actuated; and if $rank(\boldsymbol{M}) = 6$ and $N_p > 6$, the UAV is overactuated, that is, fully actuated with redundancy. The variable-tilt concepts have the advantage of converting from one class to another, since the rotors are actively tilted, and, consequently, $rank(\boldsymbol{M})$ changes.

The structure of the allowable thrust space, Λ, depends on whether the propellers have a unidirectional or bidirectional thrust-generation capability. In general, Λ can be expressed as

$$\Lambda = \{\boldsymbol{\lambda} \in \mathbb{R}^{N_p} \,|\, 0 \le \lambda_i \le \lambda_{\max} \text{ or } |\lambda_i| \le \lambda_{\max}\}, \tag{8}$$

depending on whether the ith propeller is unidirectional or bidirectional for $1 \le i \le N_p$, with the assumption that all of the propellers have the same thrust-generation capabilities and that bidirectional rotors are symmetric in the maximum thrust they produce, which is common in practice. The allowable aerodynamic-wrench space, $\mathbb{W}$, is simply the image of Λ under map $\boldsymbol{M}$. When $\mathbb{W}$ is large enough that the UAV is able to produce an aerodynamic wrench that fully counteracts gravity in any direction in Ψ_B, the UAV is classified as an omnidirectional vehicle.

Optimization-Based Design

As seen in the derivation of the control-allocation matrix, $\boldsymbol{M}$, in (6), $\boldsymbol{M}$ is uniquely defined by the rotor-configuration variables in (1). These variables are usually determined by a number of design parameters, depending on the UAV design concept, that can be produced by optimizing certain criteria. As will be covered in the "Discussion and Conclusions" section, some of these optimization criteria use properties of the mapping matrix, $\boldsymbol{M}$, since it determines the allowable control-wrench space, $\mathbb{W}$.

It must be noted that (7), which determines the control wrench, is based on a static analysis that does not take into account the UAV's inertial parameters, that is, the UAV's total mass, m, and inertia matrix, $\boldsymbol{J}$. These parameters can significantly affect the optimization process of a UAV's design for a given application. However, including the inertial parameters in the optimization process requires an analytical parametrization of $\boldsymbol{J}$ in terms of the rotors' configuration variables in (1), which increases the complexity of the design process.

Fixed-Tilt UAV Concepts

In this section, we survey fixed-tilt multirotor UAV designs, classified into nine concepts as listed in Table 1.

Each fixed-tilt concept is displayed in Figure 2 with an illustrative plot of its rotor configurations. Table 2 presents the concepts' mapping-matrix variables, including the rotor displacements, $\boldsymbol{\xi}_i$; orientations, $\boldsymbol{u}_i$; rotation direction, α_i; and design parameters for different versions of the concepts.

Quad4Hor

The first concept is an extension of a conventional quadrotor that achieves full actuation by adding four (unidirectional) horizontal rotors (indexed 5–8). There have been two different implementations of this concept in the literature. In Frankenberg and Nokleby [6], the additional rotors are positioned between the quadrotor rotor arms, as shown in Figure 2(a). The added rotors do not create a moment around the CoM, and the airflow interference among the rotors is minimized. The other implementation is by Salazar et al. [7], where the horizontal rotors are located under the vertical ones. However, the airflow interference in the design of [7] has negative effects on the controllability of the UAV. It is worth mentioning that [7] was one of the earliest attempts to obtain horizontal actuation with a multirotor UAV.

Several fully actuated multirotor platforms were introduced during the past decade to overcome the underactuation property of conventional multirotors.

Table 1. The abbreviations used in the "Fixed-Tilt UAV Concepts" and "Variable-Tilt UAV Concepts" sections.

Concept	Abbreviation
Quadrotor with four horizontal rotors	Quad4Hor
Hexarotor with canted rotors	HexC
Hexarotor with canted and dihedral rotors	HexCD
Coaxial hexagon with 12 canted rotors	CoHexC
Double tetrahedron hexarotor	HexDTet
Heptarotor with minimized frame	HeptF
Heptarotor with maximized wrench	HeptW
Octarotor cube	OctCu
Octarotor beam	OctB
Quadrotor with variable cant rotors	QuadvC
Quadrotor with variable dihedral rotors	QuadvD
Quadrotor with variable cant and dihedral rotors	QuadvCD
Quadrotor with coupled variable cant and dihedral rotors	QuadvCDc
Hexarotor with variable cant rotors	HexvC
Hexarotor with coupled variable cant rotors	HexvCc

HexC

The HexC concept [Figure 2(b)] can be considered the simplest modification of conventional multirotors to achieve fully actuated flight. The rotor's positioning is the same as the conventional hexarotor's, with all six rotors placed on the vertices of a planar hexagon. Full actuation is achieved by tilting the rotors around the axis collinear with the rotor arm. This tilting, denoted by α, is referred to as *canting*, as discussed in the "Coordinate Frames" section. By canting the rotors, they will produce thrust vertically and horizontally. The canting angle of all of the rotors is equal, and the rotors' canting and rotation directions alternate (Table 2), resulting in three symmetric rotor pairs with opposite rotation directions. Due to the design's symmetry, the drag torque of the rotors is counteracted. The amount of canting depends on the application: a large cant angle leads to high horizontal forces, while a small one results in higher flying efficiency. The angle is limited by the minimum required upward thrust for overcoming gravity.

This concept was proposed by Voyles et al. [8], [9] and achieved fully actuated flight with a cant angle of $\alpha = 20°$. The same authors demonstrated in [10] that the HexC concept has better disturbance–rejection capabilities against lateral wind gusts than the conventional hexarotor. A higher cant angle of 47° was used by Rashad et al. [11] to maximize the horizontal force applied during a contact-based scenario. An experimental 2-kg HexC platform was able to apply 1 kg of force to a vertical surface without pitching. Omnidirectional versions of the HexC concept have been proposed in [12] and [13]. In [12], a version with a cant angle optimized for a maximum wrench was proposed as a cobot for space applications. Due to the absence of gravity during the intended operation, the optimal cant angle was higher: 55° instead of the 47° in [11]. Finally, another omnidirectional version was proposed in [13] that utilized variable-pitch propellers to generate bidirectional thrust, unlike the previously presented designs, which use fixed-pitch unidirectional propellers.

HexCD

The HexCD concept, displayed in Figure 2(c), is considered an extension of the HexC. In this design, the rotors are canted and tilted along the axis perpendicular to the rotor arms, which is called a *dihedral angle* (β), as discussed in the "Coordinate Frames" section. This concept is the most studied/used design in the literature so far, with different angles optimized for different criteria. The concept was proposed by Rajappa et al. [14] who chose α and β to minimize the required total thrust for full-pose UAV controllability for a given trajectory. The optimal angles depend heavily on the trajectory; for instance, for an in-hover pitching maneuver, the optimal dihedral angle was shown to be nonzero. It was demonstrated in [14] that the direction of the dihedral angle (positive or

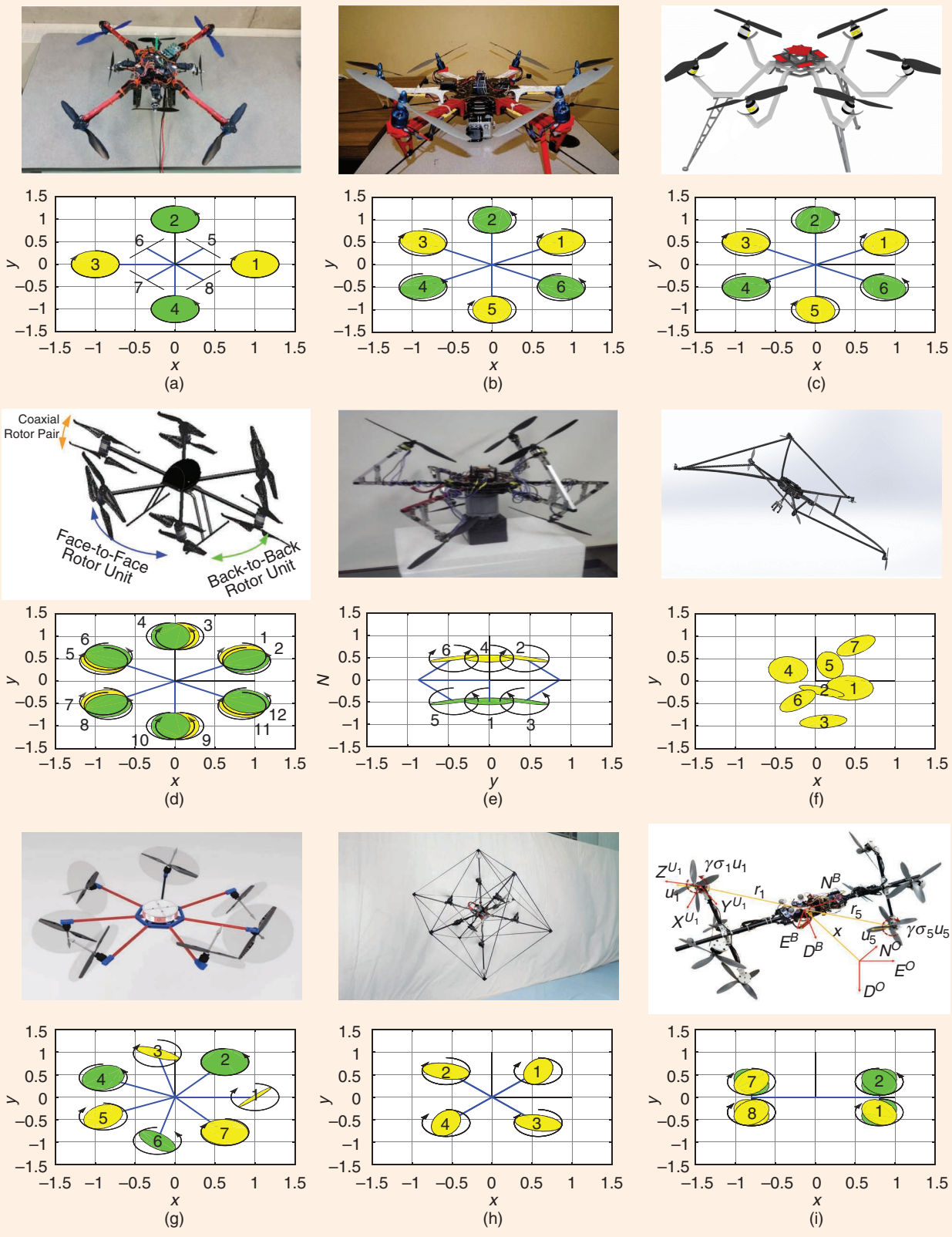

Figure 2. The fixed-tilt concepts. Each concept is accompanied by an illustration of the top/side view of the rotor configuration. Clockwise-rotating rotors are yellow, while counterclockwise ones are green. The (a) Quad4Hor [6], (b) HexC [9], (c) HexCD [14], (d) CoHexC [22], (e) HexDTet [23], (f) HeptF [25], (g) HeptW [26], (h) OctCu [27], and (i) OctB [29].

Table 2. The mapping-matrix variables for fixed-tilt concepts.

Concept	Index (i)	Rotation Direction (σ_i)	Orientation (u_i)	Displacement (ξ_i)	Fixed Parameters	Design Parameters
Quad4Hor	$1 \le i \le 4$	$\sigma_1 = \sigma_3 = 1$, $\sigma_2 = \sigma_4 = -1$	$u_i = (0, 0, 1)$	$\xi_i = (Lc_{\psi_i}, Ls_{\psi_i}, 0)$	$\psi_i = (i-1)\frac{\pi}{2}$	[6]: $\tilde{L} = \frac{L}{2}$, $\tilde{\psi} = 45^\circ$
	$5 \le i \le 8$	$\sigma_5 = \sigma_6 = 1$, $\sigma_7 = \sigma_8 = -1$	$u_i = (c_{\psi_i}, s_{\psi_i}, 0)$	$\xi_i = (\tilde{L}c_{\psi_i}, \tilde{L}s_{\psi_i}, 0)$	$\psi_i = (i-1)\frac{\pi}{2} + \tilde{\psi}$	[7]: $\tilde{L} = L$, $\tilde{\psi} = 0^\circ$
HexC	$1 \le i \le 6$	$\sigma_i = (-1)^{i+1}$	$u_i = (s_{\psi_i}s_{\alpha_i}, -c_{\psi_i}s_{\alpha_i}, c_{\alpha_i})$	$\xi_i = (Lc_{\psi_i}, Ls_{\psi_i}, 0)$	$\psi_i = (i-1)\frac{\pi}{3} + \frac{\pi}{6}$, $\alpha_i = \tilde{\alpha}(-1)^{i+1}$	[8]: $\tilde{\alpha} = 20^\circ$ [11]: $\tilde{\alpha} = 47^\circ$ [12]: $\tilde{\alpha} = 55^\circ$
HexCD	$1 \le i \le 6$	$\sigma_i = (-1)^{i+1}$	$u_i = (c_{\psi_i}s_{\beta_i} + s_{\psi_i}s_{\alpha_i}c_{\beta_i}, s_{\psi_i}s_{\beta_i} - c_{\psi_i}s_{\alpha_i}c_{\beta_i}, c_{\alpha_i}c_{\beta_i})$	$\xi_i = (Lc_{\psi_i}, Ls_{\psi_i}, 0)$	$\psi_i = (i-1)\frac{\pi}{3} + \frac{\pi}{6}$, $\alpha_i = \tilde{\alpha}(-1)^{i+1}$, $\beta_i = \tilde{\beta}$	[11]: $\tilde{\alpha} = 30^\circ$, $\tilde{\beta} = 10^\circ$ [19]: $\tilde{\alpha} = 28^\circ$, $\tilde{\beta} = 0^\circ$ [20]: $\tilde{\alpha} = 35^\circ$, $\tilde{\beta} = 0^\circ$ [32]: $\tilde{\alpha} = 47^\circ$, $\tilde{\beta} = 0^\circ$
CoHexC	$1 \le i \le 12$	$\sigma_i = (-1)^{i+1}$	$u_i = (s_{\psi_i}s_{\alpha_i}, -c_{\psi_i}s_{\alpha_i}, c_{\alpha_i})$	$\xi_i = (Lc_{\psi_i}, Ls_{\psi_i}, 0)$	$\psi_i = (i-1)\frac{\pi}{3} + \frac{\pi}{6}$, $\alpha_i = \tilde{\alpha}(-1)^{i+1}$	[22]: $\tilde{\alpha} = ?$
HexDTet	$1 \le i \le 6$	$\sigma_i = (-1)^{i}$	$u_i = (c_{\psi_i}c_{\eta}, s_{\psi_i}c_{\eta}, s_{\eta})$	$\xi_i = (Lc_{\psi_i}, Ls_{\psi_i}, (-1)^{i+1}Ls_{\eta})$	$\psi_i = (i-1)\frac{\pi}{3}$	[23]: $\eta = 75^\circ$
HeptF	$1 \le i \le 7$	$\sigma_i = 1$	$u_1 = (0.08, 0.39, 0.92)$ $u_2 = (-0.33, -0.90, 0.29)$ $u_3 = (0.13, -0.87, -0.48)$ $u_4 = (0.56, 0.08, 0.82)$ $u_5 = (0.83, 0.11, -0.55)$ $u_6 = (-0.66, 0.57, -0.49)$ $u_7 = (-0.59, 0.62, -0.51)$	$\xi_i 1 = (0.43, -0.15, -0.44)$ $\xi_i 2 = (0.08, -0.22, -0.14)$ $\xi_i 3 = (0.1, -0.9, -0.2)$ $\xi_i 4 = (-0.34, 0.25, 0.006)$ $\xi_i 5 = (0.184, 0.359, -0.254)$ $\xi_i 6 = (-0.22, -0.44, -0.04)$ $\xi_i 7 = (0.51, 0.79, -0.06)$		
HeptW	$1 \le i \le 7$	$\sigma_i = (-1)^{i+1}$	$u_1 = (-0.71, 0.67, 0.11)$ $u_2 = (0.11, 0.04, -0.98)$ $u_3 = (0.41, 0.85, 0.31)$ $u_4 = (0.44, -0.35, 0.81)$ $u_5 = (0.57, -0.38, -0.72)$ $u_6 = (-0.64, -0.58, -0.48)$ $u_7 = (-0.17, -0.26, 0.94)$	$\xi_i = (Lc_{\psi_i}, Ls_{\psi_i}, 0)$	$\psi_i = (i-1)\frac{2\pi}{7}$	
OctCu	$1 \le i \le 8$	$\sigma_i = 1$	$u_1 = u_8 = (-a, b, c)$ $u_2 = u_7 = (b, a, -c)$ $u_3 = u_6 = (-b, -a, c)$ $u_4 = u_5 = (a, -b, c)$	$\xi_i 1 = -\xi_i 8 = (d, d, d)$ $\xi_i 2 = -\xi_i 7 = (-d, d, d)$ $\xi_i 3 = -\xi_i 6 = (d, -d, d)$ $\xi_i 4 = -\xi_i 5 = (-d, -d, d)$	$a = 1/2 + 1/\sqrt{12}$ $b = 1/2 - 1/\sqrt{12}$ $c = 1/\sqrt{3}$ $d = 0.577$ m	
OctB	$1 \le i \le 8$	$\sigma_1 = \sigma_6 = 1$ $\sigma_7 = \sigma_8 = 1$ $\sigma_2 = \sigma_3 = -1$ $\sigma_4 = \sigma_5 = -1$	$u_1 = u_5 = (a, b, a)$ $u_2 = u_6 = (a, b, -a)$ $u_3 = u_7 = (a, -b, a)$ $u_4 = u_8 = (a, -b, -a)$	$\xi_i 1 = -\xi_i 5 = (L_1, -L_2, L_2)$ $\xi_i 2 = -\xi_i 6 = (L_1, L_2, L_2)$ $\xi_i 3 = -\xi_i 7 = (L_1, -L_2, -L_2)$ $\xi_i 4 = -\xi_i 8 = (L_1, L_2, -L_2)$	$a = 0.68$ $b = 0.28$ $L_1 = 0.4$ m $L_2 = 0.17$ m	

negative) does not influence the performance of the UAV. However, the maximum dihedral angle is more limited by the UAV's frame when the rotor is tilted inward ($\beta < 0$); thus, all of the rotors are tilted outward ($\beta > 0$).

The HexCD concept was also used for physical interaction in [15] and [16], with angles of $\alpha = 30^\circ$ and $\beta = 10^\circ$. Another study [17] analyzed how different angles changed the maximum achievable lateral accelerations as well as the dynamic maneuverability of the UAV. In [18] and [19], a multiobjective optimization was performed to determine the cant and dihedral angles for a physical-interaction application. The objective function was chosen as a weighted sum of three

criteria: the maximum lateral forces, flying efficiency, and dihedral effect. The interesting result in [18] and [19] was that the optimal set of angles could be chosen in most cases such that $\beta = 0$. A similar result was achieved in [20] using the dynamic maneuverability as the optimization criteria. In such a case, the HexCD concept becomes equivalent to the HexC discussed previously.

The reason for favoring $\beta = 0$ is related to the fact that a nonzero dihedral angle causes part of the generated thrust to be transformed into internal stresses in the $\hat{\boldsymbol{x}}_{p_i}$ axis. Consequently, the torque contribution of the rotor (mainly around the $\hat{\boldsymbol{z}}_B$ axis) is reduced, and so is the UAV's maneuverability. This implies that the HexC concept has greater maneuverability than the HexCD concept. However, a recent study [21] proved that a nonzero β provides the HexCD concept with robustness against rotor failure, a feature that a HexC UAV does not have.

CoHexC

This concept [Figure 2(d)], by Lei et al. [22], consists of 12 rotors positioned in pairs in a hexagonal configuration. They are called *coaxial rotor pairs* because the rotors rotate around the same axis. Both rotors rotate at the same speed but in opposite directions, and the drag torque from one rotor is counteracted by the other. The advantage of coaxial rotor pairs is that, compared to a single rotor, the amount of thrust that can be produced increases. As for the airflow interference between the top and bottom rotor, the drawbacks are less severe in this design (and for coaxial rotors in general) compared to the Quad4Hor design in [7] since both rotors have the same speed. Preliminary experiments on a test rig were carried out in [22], but, unfortunately, the authors did not provide the rotors' cant angle.

HexDTet

This concept, proposed by Toratani [23], can be considered the first attempt to produce a hexarotor with noncoplanar rotors. The design consists of six rotors restricted to the shape of two opposite tetrahedrons, as depicted in Figure 2(e). Both tetrahedrons have a common base, which lies in the $\hat{\boldsymbol{x}}_B$-$\hat{\boldsymbol{y}}_B$ plane. Each rotor is attached to an edge of the tetrahedrons, and the design parameter is the elevation angle, η, which is the angle between the common base and edge that contains a rotor. All of the rotors have the same elevation angle, which is evident in Figure 2(e). As mentioned in Table 2, the elevation angle, η, in [23] was 75°. That choice was based on an optimization process; however, the authors of [23] didn't provide any details on the optimization criteria. The work of designing noncoplanar hexarotors was also studied in [24], in which the dynamic maneuverability and maximum lateral-translations measures were used to compute the optimal configurations of the three rotor pairs.

HeptF

The UAV concept proposed by Nikou et al. [25] and presented in Figure 2(f) was one of the first attempts in the literature to create an omnidirectional UAV with only unidirectional rotors. It was shown mathematically that a minimum of seven rotors was required to achieve this. The rotor configurations were optimized to minimize the volume of the frame. Interference of the rotors' airflow was avoided by imposing a minimum distance between rotors. The distance was determined empirically based on a computational fluid dynamics analysis. Since no symmetry requirements were imposed on the UAV, all of the rotors were designed to rotate clockwise.

HeptW

The concept [Figure 2(g)] proposed by Tognon and Franchi [26] is another omnidirectional UAV with seven unidirectional rotors, similar to the HeptF concept. The rotors are placed on the vertices of a heptagon in the horizontal plane and spin in alternating directions. Their orientation is optimized for maximum omnidirectional wrench generation. This UAV concept was introduced in [26], but an operational prototype has not been developed.

OctCu

The concept [Figure 2(h)] designed by Brescianini and D'Andrea [27] is considered to be the first multirotor UAV to successfully perform omnidirectional flight. The rotor positions are fixed to the vertices of a cube, while the orientation of the rotors is optimized to maximize the vehicle's agility, measured by the maximum attainable omnidirectional wrench. All of the rotors are designed to turn in the same direction, and symmetric propellers provide bidirectional thrust. The UAV is surrounded by a cage-like frame to facilitate human–robot interaction without the risk of injury from the propellers. A detailed analysis of the proposed UAV concept and prototype can be found in [28].

To achieve full actuation, the orientation and location of the rotors must be altered, which results in a wide range of possible configurations.

OctB

Developed by Park et al. [29] and detailed in Figure 2(i), this concept is an omnidirectional octarotor UAV with a beam-like shape. The UAV was designed for aerial physical-interaction tasks that require full wrench generation. This concept is considered a to be second-generation version of the authors' beam-like hexarotor in [30]. Each side of the beam contains four rotors placed on the vertices of a square, with rotors 1 and 6–8 spinning clockwise and rotors 2–5 turning counterclockwise. The rotor configurations are optimized for omnidirectional wrench generation, while imposing a minimum rotor distance so that airflow interference is avoided. The UAV achieves

omnidirectional flight using bidirectional rotors. The bidirectional thrust generation is achieved by stacking two unidirectional propellers in the opposite direction. Thus, the proposed OctB design contains 16 propellers. In contrast to the preliminary work in [30], the authors presented a technique in [29] to shape the wrench generation by weighing the different wrench-generation directions. The OctB concept was utilized to create a serial chain of multiple fully actuated UAVs connected by spherical joints in [31]. The highly complex system performed several experimental dexterous manipulation tasks.

Variable-Tilt UAV Concepts

In this section, we survey six variable-tilt multirotor concepts, illustrated in Figure 3. The mapping-matrix variables appear in Table 3.

QuadvC

Ryll et al. [33] introduced this concept [Figure 3(a)]. Full actuation was achieved by adding four tilting actuators to a conventional quadrotor's rotors. The actuators actively canted each rotor individually around the $\hat{\boldsymbol{x}}_{P_i}$ axis. Since the rotors the authors used were unidirectional and the tilting actuators had maximum limits, the UAV's top achievable pitch/roll angle during hovering was limited to approximately 30°.

QuadvD

This concept [Figure 3(b)], by Badr et al. [34], resembles the QuadvC presented in the previous section. Instead of the cant angle, the dihedral angle is actively tiled by an extra actuator. In contrast to the cant angle, the inward dihedral angle is limited by the frame, which interferes with the rotor blades at large dihedral angles. Another difference with variable cant

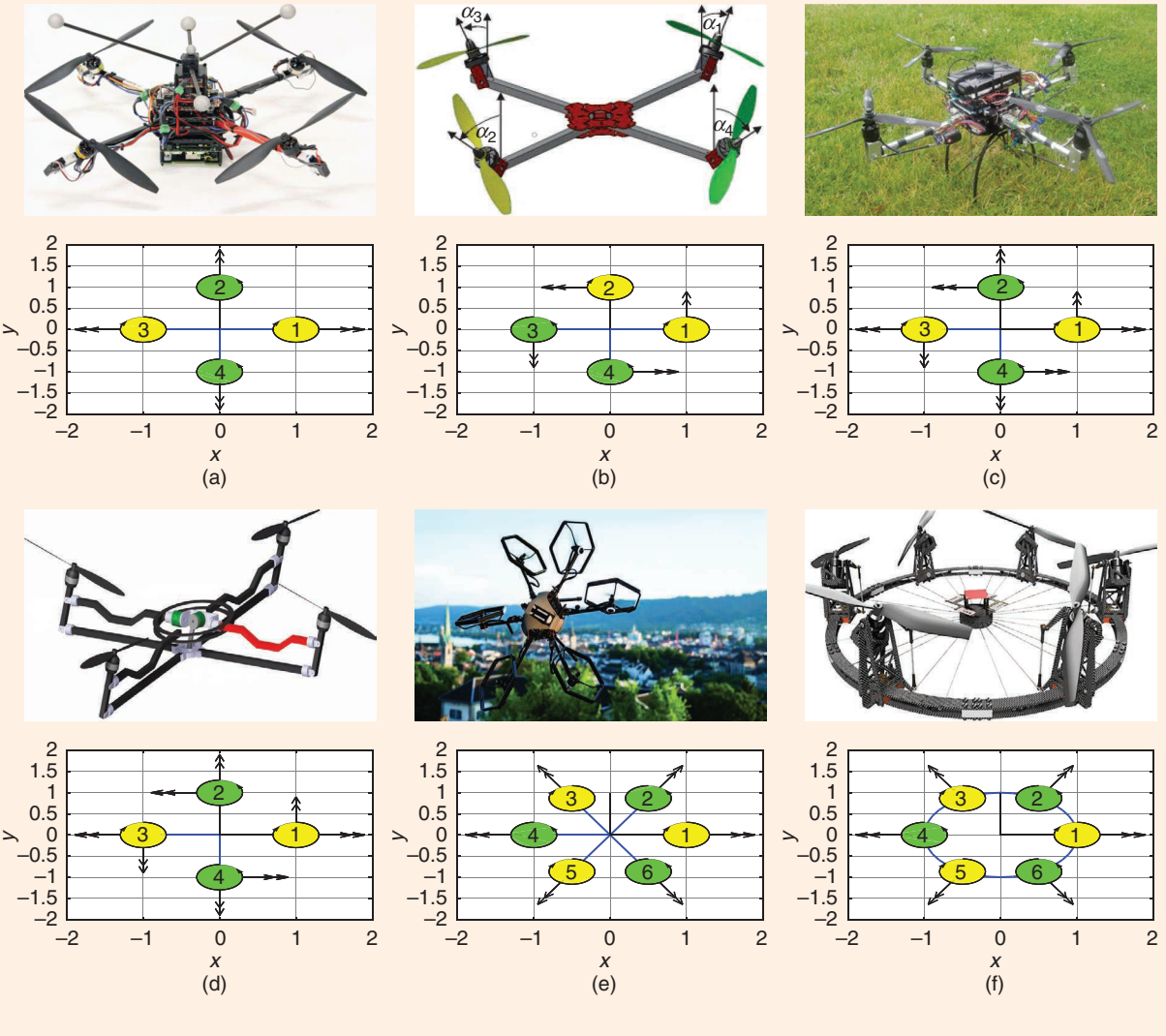

Figure 3. The variable-tilt concepts. Each concept is accompanied by an illustration of the top view of the rotor configuration. Clockwise-rotating rotors are yellow, while counterclockwise ones are green. Double arrows indicate the active tilt axis. The (a) QuadvC [36], (b) QuadvD [34], (c) QuadvCD [35], (d) QuadvCDc [37], (e) HexvC [38], and (f) HexvCc [40].

Table 3. The mapping-matrix variables for variable-tilt concepts.

Concept	Index (i)	Rotation Direction (σ_i)	Orientation (u_i)	Displacement (ξ_i)	Fixed Parameters	Active Tilt
QuadvC	$1 \le i \le 4$	$\sigma_i = (-1)^{i+1}$	$u_i = (s_{\psi_i} s_{\alpha_i}, -c_{\psi_i} s_{\alpha_i}, c_{\alpha_i})$	$\xi_i = (Lc_{\psi_i}, Ls_{\psi_i}, 0)$	$\psi_i = (i-1)\frac{\pi}{2}$	α_i
QuadvD	$1 \le i \le 4$	$\sigma_1 = \sigma_2 = 1$ $\sigma_3 = \sigma_4 = -1$	$u_i = (c_{\psi_i} s_{\beta_i}, s_{\psi_i} s_{\beta_i}, c_{\beta_i})$		$\psi_i = (i-1)\frac{\pi}{2}$	β_i
QuadvCD	$1 \le i \le 4$	$\sigma_i = (-1)^{i+1}$	$u_i = (c_{\psi_i} s_{\beta_i} + s_{\psi_i} s_{\alpha_i} c_{\beta_i},$ $s_{\psi_i} s_{\beta_i} - c_{\psi_i} s_{\alpha_i} c_{\beta_i}, c_{\alpha_i} c_{\beta_i})$		$\psi_i = (i-1)\frac{\pi}{2}$	α_i β_i
QuadcCDc	$1 \le i \le 4$				$\psi_i = (i-1)\frac{\pi}{2}$ $\alpha_1 = -\alpha_3 = \alpha_m$ $\alpha_2 = -\alpha_4 = \beta_m$ $\beta_1 = -\beta_3 = \beta_m$ $\beta_2 = -\beta_4 = -\alpha_m$	α_m β_m
HexvC	$1 \le i \le 6$	$\sigma_i = (-1)^{i+1}$	$u_i = (s_{\psi_i} s_{\alpha_i}, -c_{\psi_i} s_{\alpha_i}, c_{\alpha_i})$	$\xi_i = (Lc_{\psi_i}, Ls_{\psi_i}, 0)$	$\psi_i = (i-1)\frac{\pi}{3}$	α_i
HexvCc	$1 \le i \le 6$				$\psi_i = (i-1)\frac{\pi}{3}$ $\alpha_i = \alpha_m (-1)^{i+1}$	α_m

rotors is that the dihedral angle does not contribute to the yaw torque (as discussed in the section "HexCD"), effectively reducing the total torque.

QuadvCD

This concept by Segui-Gasco et al. [35] [Figure 3(c)] combines the approaches presented in the two previous sections. Two actuators added to each rotor of a conventional quadrotor actively tilt the rotors around the cant and dihedral angles. Thus, the UAV has eight actuators for the thrust vectoring. For the dihedral tilt actuation, the push–pull mechanism used limited the maximum achievable dihedral angle. However, an alternative actuation method for the cant and dihedral tilting that can be used to extend the range of achievable cant and dihedral angles was proposed by Ryll et al. in [36].

QuadvCDc

In this concept [Figure 3(d)], Odelga et al. [37] proposed to actuate the angle of all quadrotor propellers by using a single actuator with a parallelogram linkage mechanism instead of actuating each rotor separately. This linkage mechanism tilts all of the rotors in the same direction. For a second rotation direction, a similar linkage is used. In this way, the rotors have the same orientation and cannot be orientated individually, in contrast to the QuadvCD concept. One drawback of such a coupling feature is that the maximum tilting angle of the rotors in all directions is limited by the maximum inward dihedral angle. The main advantage of this actuation method is that it reduces the number of actuators required for the cant and dihedral actuation from eight to two. In [37], only a conceptual proposition of the design was provided, and a working prototype has not been reported.

Table 4. The optimization criteria for designing fixed-tilt concepts.

Optimization Criteria	References
Maximum allowed wrench	[12], [18], [19], [32], [26], [28], [29]
Maximum allowed accelerations	[17], [24]
Minimum control effort	[14]
Maximum flying efficiency	[18], [19]
Minimum dihedral effect	[19]
Maximum dynamic maneuverability	[20], [24]
Minimum volume of vehicle	[25]

HexvC

Shown in Figure 3(e) and presented in [38], this is the first variable-tilt concept to achieve successful omnidirectional flight. It contains a canting actuator added to each rotor of a conventional hexarotor to achieve omnidirectional flight with unidirectional thrust generation. The UAV was developed by a group of students at the Swiss Federal Institute of Technology, Zurich, and Zurich University of the Arts. A modified version was proposed in [39] for contact-based aerial-inspection applications. The UAV design in [39] had coaxial rotors to increase the thrust-generation capabilities of the UAV, with all other design aspects remaining the same.

HexvCc

Finally, the concept by Ryll et al. [40] [Figure 3(f)] uses a single actuator to cant all of a hexarotor's rotors. This coupled rotor tilting is achieved through a wire mechanism. The cant

angle alternates similarly to that in the HexC concept, while the maximum achievable cant angle is limited by the frame. The advantage of a single actuator instead of six to cant the rotors is that the energy consumption and total mass of the system are greatly reduced compared to the parallel mechanism of the QuadvCDc concept. However, the maneuverability of the UAV is reduced by the lower bandwidth of the tilting mechanism that uses wires.

Discussion and Conclusions

In this article, we reviewed multirotor UAV concepts proposed in the literature over the past decade. The concepts were classified into fixed- and variable-tilt UAVs in which the mapping matrix is structurally different. The design variables for reconstructing the concepts' mapping matrices were provided as well. We conclude with some remarks on different issues related to the work.

The HexC and HexCD concepts are found most widely in the literature, which is a consequence of their mechanical simplicity and the ease of transforming the conventional hexarotor into a fully actuated vehicle. Due to a low number of design parameters, these concepts reduce the effort of optimizing designs for a given application. Different fixed-tilt designs were optimized based on a variety of criteria, as summarized in Table 4. The most-used measure maximizes the control wrench generated with (7) in specific directions or all directions (for omnidirectional UAVs). However, it is important to know that (7) is based on a static analysis and does not take into account the UAV's inertia parameters, such as the dynamic-maneuverability and generated control acceleration measures. As an example of the false intuition these criteria can provide, the maximum wrench of the CoHexC concept would be twice that of the HexC design (assuming that the propellers and cant angle were identical). However, considering that the CoHexC has (roughly) double the inertia parameters of the HexC, the maximum acceleration is (approximately) the same.

We close with a remark about the control-system architecture of the presented UAVs. In most of the works surveyed here, a two-stage control architecture is employed, where the control wrench from (7) is considered a virtual input to the rigid body model of the UAV and the mapping matrix is used to compute the desired propeller thrusts. For fixed-tilt concepts, this involves computing the inverse/pseudo-inverse of the $\boldsymbol{M}$ matrix, which is guaranteed to exist, as shown in the "HexCD" section. However, for variable-tilt designs, the control-allocation problem is more involved, as the rank of the $\boldsymbol{M}$ matrix might change during flight and the UAV might operate in an underactuated configuration. This calls for nonlinear control-allocation techniques and control algorithms that can handle different UAV operating conditions, such as those in [41].

Acknowledgment

This work was funded by the INTERREG Deutschland–Nederland cooperation program as part of SPECTORS project 143081.

References

[1] F. Ruggiero, V. Lippiello, and A. Ollero, "Aerial manipulation: A literature review," *IEEE Robot. Autom. Lett.*, vol. 3, no. 3, pp. 1957–1964, July 2018. doi: 10.1109/LRA.2018.2808541.

[2] R. Austin, *Unmanned Aircraft Systems: UAVS Design, Development and Deployment*. Hoboken, NJ: Wiley, 2010.

[3] K. Valavanis and G. J. Vachtsevanos, Eds., *Handbook of Unmanned Aerial Vehicles*. Berlin: Springer-Verlag, 2015.

[4] S. Stramigioli, *Modeling and IPC Control of Interactive Mechanical System—A Coordinate-Free Approach*. London: Springer-Verlag, 2001.

[5] R. Mahony, V. Kumar, and P. Corke, "Multirotor aerial vehicles," *IEEE Robot. Autom. Mag.*, vol. 20, no. 32, pp. 20–32, Sept. 2012. doi: 10.1109/MRA.2012.2206474.

[6] F. von Frankenberg and S. Nokleby, "Disturbance rejection in multirotor unmanned aerial vehicles using a novel rotor geometry," in *Proc. 4th Int. Conf. Control Dynamic Systems and Robotics*, 2017. doi: 10.11159/cdsr17.130.

[7] S. Salazar, H. Romero, R. Lozano, and P. Castillo, "Modeling and real-time stabilization of an aircraft having eight rotors," *J. Intell. Robot. Syst.*, vol. 54, no. 1–3, pp. 455–470, Mar. 2009. doi: 10.1007/s10846-008-9274-x.

[8] R. Voyles and G. Jiang, "Hexrotor UAV platform enabling dextrous interaction with structures—Preliminary work," in *Proc. 2012 IEEE Int. Symp. Safety, Security, and Rescue Robotics (SSRR)*. doi: 10.1109/SSRR.2012.6523891.

[9] G. Jiang and R. Voyles, "Hexrotor UAV platform enabling dextrous interaction with structures—Flight test," in *Proc. 2013 IEEE Int. Symp. Safety, Security, and Rescue Robotics (SSRR)*. doi: 10.1109/SSRR.2013.6719377.

[10] G. Jiang and R. Voyles, "A nonparallel hexrotor UAV with faster response to disturbances for precision position keeping," in *Proc. 2014 IEEE Int. Symp. Safety, Security, and Rescue Robotics (SSRR)*. doi: 10.1109/SSRR.2014.7017669.

[11] R. Rashad, J. B. Engelen, and S. Stramigioli, "Energy tank-based wrench/impedance control of a fully-actuated hexarotor: A geometric port-Hamiltonian approach," in *Proc. 2019 Int. Conf. Robotics and Automation (ICRA)*. doi: 10.1109/ICRA.2019.8793939.

[12] P. Roque and R. Ventura, "Space CoBot: Modular design of a holonomic aerial robot for indoor microgravity environments," in *Proc. 2016 IEEE/RSJ Int. Conf. Intelligent Robots and Systems (IROS)*, pp. 4383–4390. doi: 10.1109/IROS.2016.7759645.

[13] E. Kaufman, K. Caldwell, D. Lee, and T. Lee, "Design and development of a free-floating hexrotor UAV for 6-DoF maneuvers," in *Proc. 2014 IEEE Aerospace Conf.* doi: 10.1109/AERO.2014.6836427.

[14] S. Rajappa, M. Ryll, H. H. Bülthoff, and A. Franchi, "Modeling, control and design optimization for a fully-actuated hexarotor aerial vehicle with tilted propellers," in *Proc. 2015 IEEE Int. Conf. Robotics and Automation (ICRA)*, pp. 4006–4013. doi: 10.1109/ICRA.2015.7139759.

[15] N. Staub, D. Bicego, Q. Sablé, V. Arellano-Quintana, S. Mishra, and A. Franchi, "Towards a flying assistant paradigm: The OTHex," in *Proc. 2018 IEEE Int. Conf. Robotics and Automation (ICRA)*, Brisbane, Australia, pp. 6997–7002. doi: 10.1109/ICRA.2018.8460877.

[16] M. Ryll et al., "6D physical interaction with a fully actuated aerial robot," in *Proc. 2017 IEEE Int. Conf. Robotics and Automation (ICRA)*, pp. 5190–5195. doi: 10.1109/ICRA.2017.7989608.

[17] H. Mehmood, T. Nakamura, and E. N. Johnson, "A maneuverability analysis of a novel hexarotor UAV concept," in *Proc. 2016 Int. Conf. Unmanned Aircraft Systems*, pp. 437–446. doi: 10.1109/ICUAS.2016.7502576.

[18] G. Jiang, R. Voyles, K. Sebesta, and H. Greiner, "Estimation and optimization of fully-actuated multirotor platform with nonparallel actuation mechanism," in *Proc. 2017 IEEE/RSJ Int. Conf. Intelligent Robots and Systems (IROS)*, pp. 6843–6848. doi: 10.1109/IROS.2017.8206605.

[19] G. Jiang, R. M. Voyles, and J. J. Choi, "Precision fully-actuated UAV for visual and physical inspection of structures for nuclear decommissioning and search and rescue," in *Proc. 2018 IEEE Int. Symp. Safety, Security, and Rescue Robotics (SSRR)*. doi: 10.1109/SSRR.2018.8468628.

[20] Y. Tadokoro, T. Ibuki, and M. Sampei, "Maneuverability analysis of a fully-actuated hexrotor UAV considering tilt angles and arrangement of rotors," *IFAC-PapersOnLine*, vol. 50, no. 1, pp. 8981–8986, July 2017. doi: 10.1016/j.ifacol.2017.08.1325.

[21] G. Michieletto, M. Ryll, and A. Franchi, "Fundamental actuation properties of multirotors: Force–moment decoupling and fail–safe robustness," *IEEE Trans. Robot.*, vol. 34, no. 3, pp. 702–715, June 2018. doi: 10.1109/TRO.2018.2821155.

[22] Y. Lei, Y. Ji, C. Wang, Y. Bai, and Z. Xu, "Aerodynamic design on the non-planar rotor system of a multi-rotor flying robot (MFR)," in *Proc. 2017 IEEE 3rd Int. Symp. Robotics and Manufacturing Automation (ROMA)*. doi: 10.1109/ROMA.2017.8231740.

[23] D. Toratani, "Research and development of double tetrahedron hexa-rotorcraft (DOT-HR)," in *Proc. 28th Congr. Int. Council Aeronautical Sciences (ICAS)*, 2012, pp. 1–8. [Online]. Available: http://icas.org/ICAS_ARCHIVE/ICAS2012/ABSTRACTS/727.HTM

[24] K. Kiso, T. Ibuki, M. Yasuda, and M. Sampei, "Structural optimization of hexrotors based on dynamic manipulability and the maximum translational acceleration," in *Proc. 2015 IEEE Conf. Control Applications (CCA)*, pp. 774–779. doi: 10.1109/CCA.2015.7320711.

[25] A. Nikou, G. C. Gavridis, and K. J. Kyriakopoulos, "Mechanical design, modelling and control of a novel aerial manipulator," in *Proc. 2015 IEEE Int. Conf. Robotics and Automation (ICRA)*, pp. 4698–4703. doi: 10.1109/ICRA.2015.7139851.

[26] M. Tognon and A. Franchi, "Omnidirectional aerial vehicles with unidirectional thrusters: Theory, optimal design, and control," *IEEE Robot. Autom. Lett.*, vol. 3, no. 3, pp. 2277–2282, July 2018. doi: 10.1109/LRA.2018.2802544.

[27] D. Brescianini and R. D'Andrea, "Design, modeling and control of an omni-directional aerial vehicle," in *Proc. 2016 IEEE Int. Conf. Robotics and Automation (ICRA)*, pp. 3261–3266. doi: 10.1109/ICRA.2016.7487497.

[28] D. Brescianini and R. D'Andrea, "An omni-directional multirotor vehicle," *Mechatronics*, vol. 55, pp. 76–93, Nov. 2018. doi: 10.1016/j.mechatronics.2018.08.005.

[29] S. Park et al., "ODAR: Aerial manipulation platform enabling omni-directional wrench generation," *IEEE/ASME Trans. Mechatronics*, vol. 23, no. 4, pp. 1907–1918, Aug. 2018. doi: 10.1109/TMECH.2018.2848255.

[30] S. Park, J. Her, J. Kim, and D. Lee, "Design, modeling and control of omni-directional aerial robot," in *Proc. 2016 IEEE/RSJ Int. Conf. Intelligent Robots and Systems (IROS)*, pp. 1570–1575. doi: 10.1109/IROS.2016.7759254.

[31] H. Yang, S. Park, J. Lee, J. Ahn, D. Son, and D. Lee, "LASDRA: Large-size aerial skeleton system with distributed rotor actuation," in *Proc. 2018 IEEE Int. Conf. Robotics and Automation (ICRA)*, pp. 7017–7023. doi: 10.1109/ICRA.2018.8460713.

[32] R. Rashad, P. Kuipers, J. Engelen, and S. Stramigioli, "Design, modeling, and geometric control on SE(3) of a fully-actuated hexarotor for aerial interaction," 2017. [Online]. Available: https://arxiv.org/abs/1709.05398

[33] M. Ryll, H. H. Bülthoff, and P. R. Giordano, "Modeling and control of a quadrotor UAV with tilting propellers," in *Proc. 2012 IEEE Int. Conf. Robotics and Automation (ICRA)*, pp. 4606–4613. doi: 10.1109/ICRA.2012.6225129.

[34] S. Badr, O. Mehrez, and A. E. Kabeel, "A novel modification for a quadrotor design," in *Proc. 2016 Int. Conf. Unmanned Aircraft Systems (ICUAS)*, pp. 702–710.

[35] P. Segui-Gasco, Y. Al-Rihani, H.-S. Shin, and A. Savvaris, "A novel actuation concept for a multi rotor UAV," *J. Intell. Robot. Syst.*, vol. 74, no. 1–2, pp. 173–191, Apr. 2014. doi: 10.1007/s10846-013-9987-3.

[36] M. Ryll, H. H. Bülthoff, and P. R. Giordano, "A novel overactuated quadrotor unmanned aerial vehicle: Modeling, control, and experimental validation," *IEEE Trans. Control Syst. Technol.*, vol. 23, no. 2, pp. 540–556, Mar. 2015. doi: 10.1109/TCST.2014.2330999.

[37] M. Odelga, P. Stegagno, and H. H. Bülthoff, "A fully actuated quadrotor UAV with a propeller tilting mechanism: Modeling and control," in *Proc. 2016 IEEE Int. Conf. Advanced Intelligent Mechatronics (AIM)*, pp. 306–311. doi: 10.1109/AIM.2016.7576784.

[38] M. Kamel et al., "The Voliro omniorientational hexacopter: An agile and maneuverable tiltable-rotor aerial vehicle," *IEEE Robot. Autom. Mag.*, vol. 25, no. 4, pp. 34–44, Dec. 2018. doi: 10.1109/MRA.2018.2866758.

[39] K. Bodie, Z. Taylor, M. Kamel, and R. Siegwart, "Towards efficient full pose omnidirectionality with overactuated MAVS," 2018. [Online]. Available: https://arxiv.org/abs/1810.06258

[40] M. Ryll, D. Bicego, and A. Franchi, "Modeling and control of FAST-Hex: A fully-actuated by synchronized-tilting hexarotor," in *Proc. 2016 IEEE/RSJ Int. Conf. Intelligent Robots and Systems (IROS)*, pp. 1689–1694. doi: 10.1109/IROS.2016.7759271.

[41] A. Franchi, R. Carli, D. Bicego, and M. Ryll, "Full-pose tracking control for aerial robotic systems with laterally bounded input force," *IEEE Trans. Robot.*, vol. 34, no. 2, pp. 534–541, Apr. 2018. doi: 10.1109/TRO.2017.2786734.

Ramy Rashad, Robotics and Mechatronics Group, University of Twente, Enschede, The Netherlands. Email: r.a.m.rashadhashem@utwente.nl.

Jelmer Goerres, Structural Dynamics, Acoustics, and Control Group, University of Twente, Enschede, The Netherlands. Email: jelmergoerres@gmail.com.

Ronald Aarts, Structural Dynamics, Acoustics, and Control Group, University of Twente, Enschede, The Netherlands. Email: r.g.k.m.aarts@utwente.nl.

Johan B.C. Engelen, Robotics and Mechatronics Group, University of Twente, Enschede, The Netherlands. Email: jbc.engelen@gmail.com.

Stefano Stramigioli, Robotics and Mechatronics Group, University of Twente, The Netherlands, and ITMO University, Saint Petersburg, Russia. Email: s.stramigioli@utwente.nl.